Supporting Information

Controlling Molecular Conformation for Highly Efficient and Stable Deep-Blue Copolymer Light-Emitting Diodes

Iain Hamilton,[†] Nathan Chander,[†] Nathan J. Cheetham,[†] Minwon Suh,[†] Matthew Dyson,[†,§] Xuhua Wang,[†] Paul N. Stavrinou,[‡] Michael Cass,[⊥] Donal D. C. Bradley,[‡,∥] and Ji-Seon Kim*[†]*

† Department of Physics and Centre for Plastic Electronics, Imperial College London, London SW7 2AZ, UK

‡ Department of Engineering Science, University of Oxford, Parks Road, Oxford, OX1 3PJ, UK

§ Molecular Materials and Nanosystems and Institute for Complex Molecular Systems, Eindhoven University of Technology, P.O. Box 513, 5600 MB Eindhoven, The Netherlands

⊥ Cambridge Display Technology Ltd, Unit 12 Cardinal Park, Godmanchester, Cambridgeshire PE29 2XG, UK

∥ Department of Physics and Division of Mathematical, Physical and Life Sciences, University of Oxford, 9 Parks Road, Oxford, OX1 3PD, UK

* ji-seon.kim@imperial.ac.uk, Donal.Bradley@mpls.ox.ac.uk

Contents

β-phase fraction calculation

The absorption spectra of the homopolymer (PFO), copolymer (nF8:mBSP) and blend (xPFO/yPFB) films can be described as a superposition of the absorption of disordered glassy-phase (broad peak centred at ≈ 385 nm) and well-ordered β-phase (resolved vibronic band with S_0-S_1 0-0 peak at ≈ 435 nm) chain segments. To estimate the fraction of β-phase chain segments in each film, the appropriate reference 'purely-glassy' absorption spectrum (blue dashed line in Figure S1) is fitted at 3.55 eV where there is negligible β-phase segment absorption.[S1] The thus-normalised glassy spectrum is then subtracted from the film spectrum and the residual corresponds to the β-phase chain segment absorption (red dashed line). The fraction of β-phase segments in the film can then be estimated from the ratio of the integrated absorption areas after taking into account the enhanced oscillator strength for β-phase segments (a factor of 1.08).[S1]

$$\beta\text{-phase fraction (\%)} = \frac{\Delta A}{\Delta A + \{(A_{\text{total}} - \Delta A) \times 1.08\}} \times 100$$

In the examples shown in Figure S1 we estimate (from top to bottom) 10, 5 and 12% β-phase chain segments.

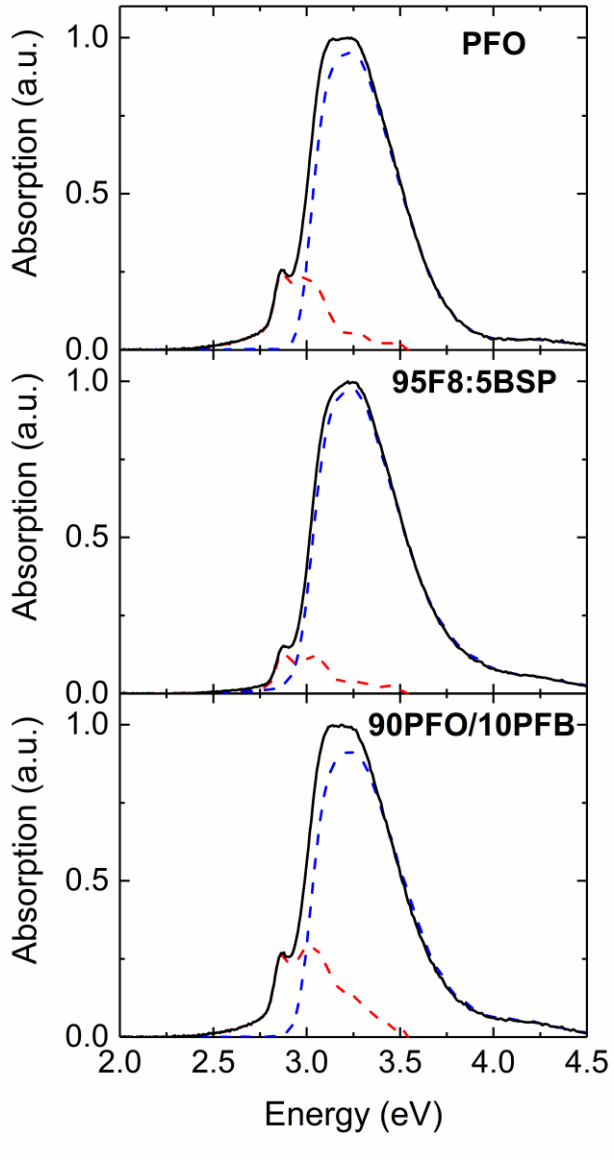

Figure S1. Normalised absorption spectra of homopolymer PFO, copolymer 95F8:5BSP and blend 90PFO/10PFB β-phase films (black solid line). In each case, a 'purely-glassy' film spectrum (blue dashed lines) is overlaid. The difference spectra correspond to the β-phase segment absorptions (red).

A higher fraction of β-phase chain segments is formed in films of the PFO homopolymer (10%) and 90PFO/10PFB blend (12%) than in films of the 95F8:5BSP copolymer (5%). The effect that PFB chains have on neighbouring PFO chain motions in blend films is difficult to predict *a priori*. Both disruptive (motion constraining) and assistive (free-volume generating) effects might occur and their balance will influence the degree to which β-phase conformations can be adopted by the PFO fraction. Further studies will be required to investigate this behaviour in detail but we note that here the overall effect of forming a blend with 10% PFB is marginally beneficial to β-phase generation. In contrast, for the 95F8:5BSP copolymer, the BSP moieties are present within all of the chains and the smaller fraction of β-phase chain segments observed following SVA then suggests that in this case they tend to impede β-phase formation.

Uv-vis and PL spectra for 97F8:3BSP, 90F8:10BSP, 80F8:20BSP and PFB copolymer films

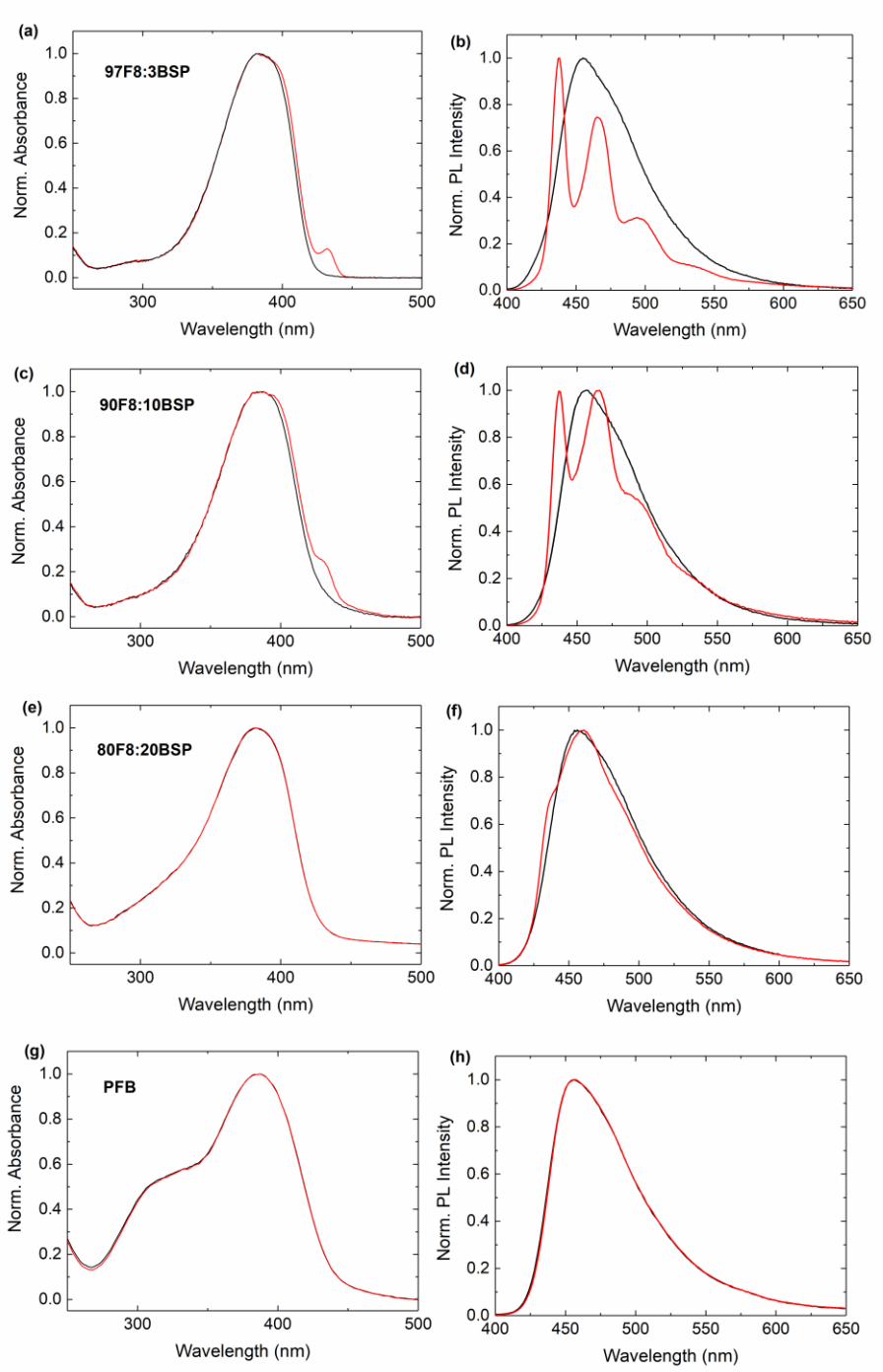

Figure S2. UV-vis absorption (left column) and PL spectra (right column) for pre- (black line) and post- (red line) solvent-vapour-annealed copolymer films of 97F8:3BSP ((a) and (b)), 90F8:10BSP ((c) and (d)), 80F8:20BSP ((e) and (f)) and 50F8:50BSP (PFB) ((g) and (h)).

Table S1. Comparison of β-phase fraction and β-phase PL contribution for solvent vapour annealed 97F8:3BSP, 90F8:10BSP, 80F8:20BSP and PFB copolymer films determined by fitting the data shown in Figure S2.

Polymer	β-phase fraction	β-phase PL contribution
97F8:3BSP	6% ± 1%	69%
90F8:10BSP	3% ± 1%	46%
80F8:20BSP	0.2% ± 0.1%	8%
PFB (50F8:50BSP)	0%	0%

The formation of β-phase chain segments was investigated for further F8:BSP statistical copolymer compositions, namely 97F8:3BSP, 90F8:10BSP and 80F8:20BSP with 3%, 10% and 20% of butyl substituted phenylenediamine (BSP) units, and for PFB, the 50F8:50BSP alternating copolymer. Figure S2 shows their thin film UV-vis and PL spectra before and after solvent vapour annealing (SVA) using the same conditions outlined in the experimental section of the main paper. The 97F8:3BSP copolymer forms 6% β-phase chain segments but this gives rise to 69% of the PL emission. SVA of the 90F8:10BSP copolymer yields a smaller fraction of β-phase segments (3%) but again, this is disproportionately represented in the emission, with a 46% β-phase PL contribution. Interestingly, the 80F8:20BSP copolymer still shows a small amount of β-phase when in fact none would be expected were the BSP units evenly distributed amongst the polymer chains. Four F8 units between each BSP unit would be too short a sequence to support β-phase segment formation. The very small (0.2%) fraction of β-phase segments is again over-represented in PL with an 8% fraction in emission. Lastly, it is confirmed that, as expected, β-phase segments cannot form in the alternating copolymer (PFB).

Solvatochromism in PFO, 95F8:5BSP and PFB

Figure S3 shows the effect of solvent polarity (toluene *vs* THF *vs* dichlorobenzene) on the solution PL spectra for PFO, PFB and 95F8:5BSP. Very small spectral shifts are seen for the vibronically structured PFO PL consistent with neutral exciton emission. For PFB the PL shifts are substantially larger, as expected for excited states with charge transfer (CT) character. For 95F8:5BSP the emission has both neutral exciton and CT-like components that show a combination of PFO- and PFB-like behaviours.

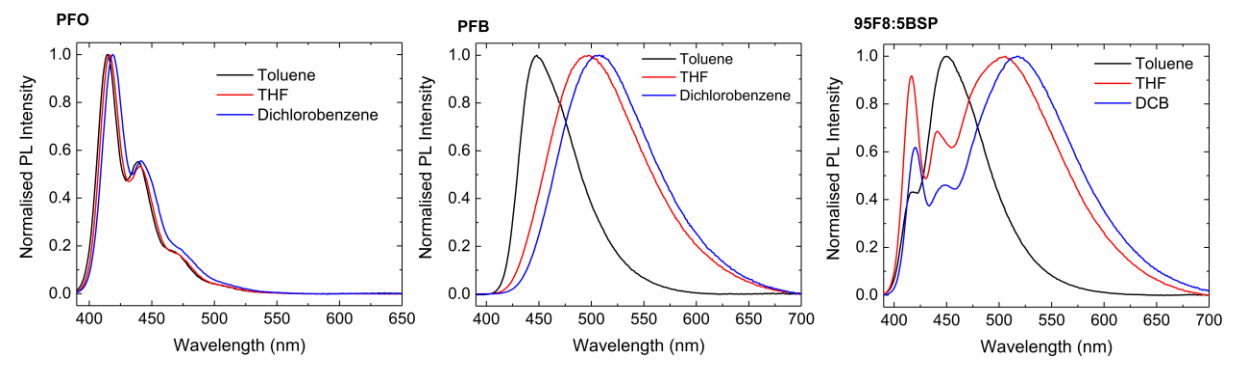

Figure S3. PL spectra of PFO, PFB and 95F8:5BSP in dilute Toluene, THF and Dichlorobenzene solutions.

Cyclic Voltammetry

For reference in the discussion of energy transfer processes occurring in the homopolymer, copolymer and blend films, the HOMO and LUMO levels of PFO, 95F8:5BSP and PFB were determined using cyclic voltammetry (CV). Films were prepared by spin coating onto ITO substrates that acted as the working electrode in a traditional three-electrode setup. A platinum wire was used as the auxiliary electrode and Ag/Ag^+ as reference electrode. The measurements (scan rate 100 mV/s) were carried out using a 0.1M tetrabutylammonium hexafluorophosphate ($TBAPF_6$) acetonitrile solution for both oxidation and reduction, and recorded using an Autolab PGSTAT101 instrument. For the CV measurements in acetonitrile, the glassware was dried at 100 °C and the cell purged with argon during the measurement to prevent oxygen contamination.

The measurement was calibrated by collecting a CV scan for ferrocene, with its known ionisation potential of 4.8 eV. The corresponding half wave potential ($E_{1/2}$) for Fe/Fe^+ was measured to be 0.40 eV in our setup, yielding:

$$E_{\mathrm{HOMO}} = (E_{\mathrm{ox}} + 4.40\ \mathrm{eV})$$

$$E_{\mathrm{LUMO}} = (E_{\mathrm{red}} + 4.40\ \mathrm{eV})$$

Where E_{ox} and E_{red} are the onset voltages for oxidation and reduction respectively.

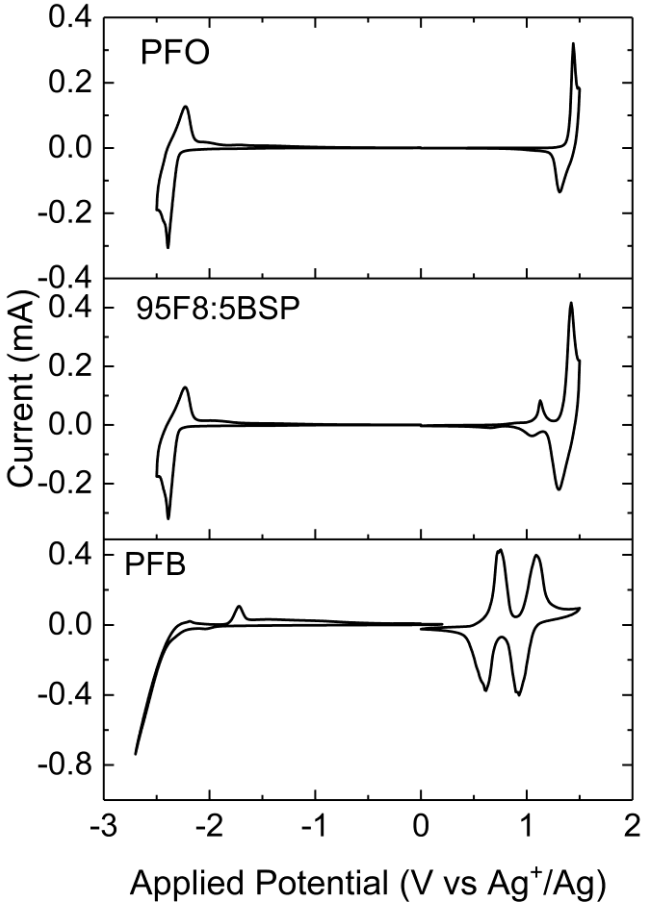

Figure S4. Cyclic voltammograms for thin film samples of (a) PFO, (b) 95F8:5BSP and (c) PFB recorded in $TBAPF_6$ acetonitrile solution.

Table S2. Table showing values of oxidation onset energy, reduction onset energy and estimated HOMO and LUMO energies for PFO, 95F8:5BSP and PFB.

Polymer	**E_{ox} (eV)**	**E_{red} (eV)**	**HOMO (eV)**	**LUMO (eV)**
PFO	1.40	-2.30	5.80	2.10
95F8:5BSP	1.09	-2.30	5.49	2.10
PFB	0.65	-2.40	5.05	2.00

A spatial separation of electron and hole wavefunctions is supported by cyclic voltammetry (CV) measurements (Figure S4). For 95F8:5BSP a small oxidation peak is observed at ~ 0.3 V below the main F8 oxidation peak. This can be assigned to preferential oxidation of BSP moieties confirming HOMO localization at these sites. Conversely, the LUMO will tend to delocalize across extended F8 sequences.[S2] The introduction of BSP moieties can thereby lead to hole trapping and enhanced exciton formation in PLEDs.[S3]

Deconvoluted photoluminescence spectra

The PL spectra were deconvoluted to determine the contribution of β-phase F8 segments to the PL emission. Here, the 95F8:5BSP copolymer and 90PFO/10PFB blend β-phase film PL were fitted by the sum of two reference PL spectra. For copolymer β-phase films the reference spectra used were: PL of glassy 95F8:5BSP (dashed red line in left panel of Figure S5) and β-phase PFO (blue dashed lines). For the 90PFO/10PFB blend film, a glassy PFB (50PFO:50BSP) reference was used (red dashed line in right panel of Figure S5) along with the same β-phase PFO spectrum.

The relative magnitudes of the reference spectra were adjusted so that the sum (black solid line in Figure S5) gave a good fit to the measured β-phase PL spectra (open circles). The relative contribution of the β-phase emission was then found from the ratio of the integrated intensities.

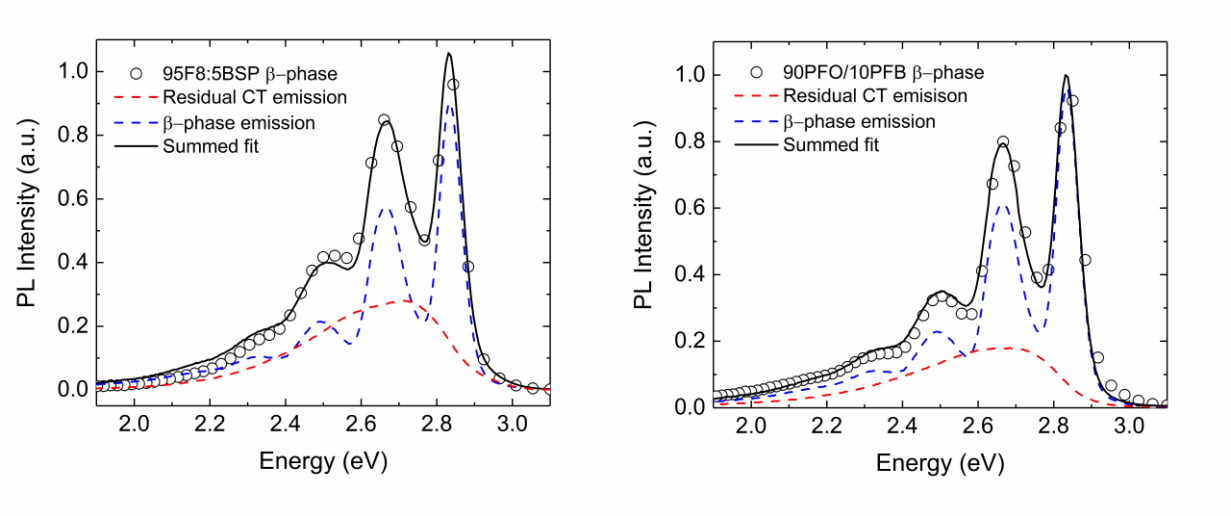

Figure S5. Deconvolution of PL spectra for 95F8:5BSP copolymer β-phase sample (left – open circles) and 90PFO/10PFB blend β-phase sample (right – open circles). The red dashed line shows residual PFB-like CT emission whilst the blue dashed line shows the vibronic β-phase emission. The solid black line shows the combined sum of residual CT and β-phase emissions. The fractional contribution from each component was deduced by integration over their deconvoluted spectra.

For the copolymer, the β-phase fraction accounted for 62% of total emission whilst for the blend, β-phase PFO emission accounted for 82% of the total spectra.

Overlaid UV-vis absorbance and photoluminescence spectra for glassy- and β-phase PFO, 95F8:5BSP copolymer and 90PFO/10PFB blend films

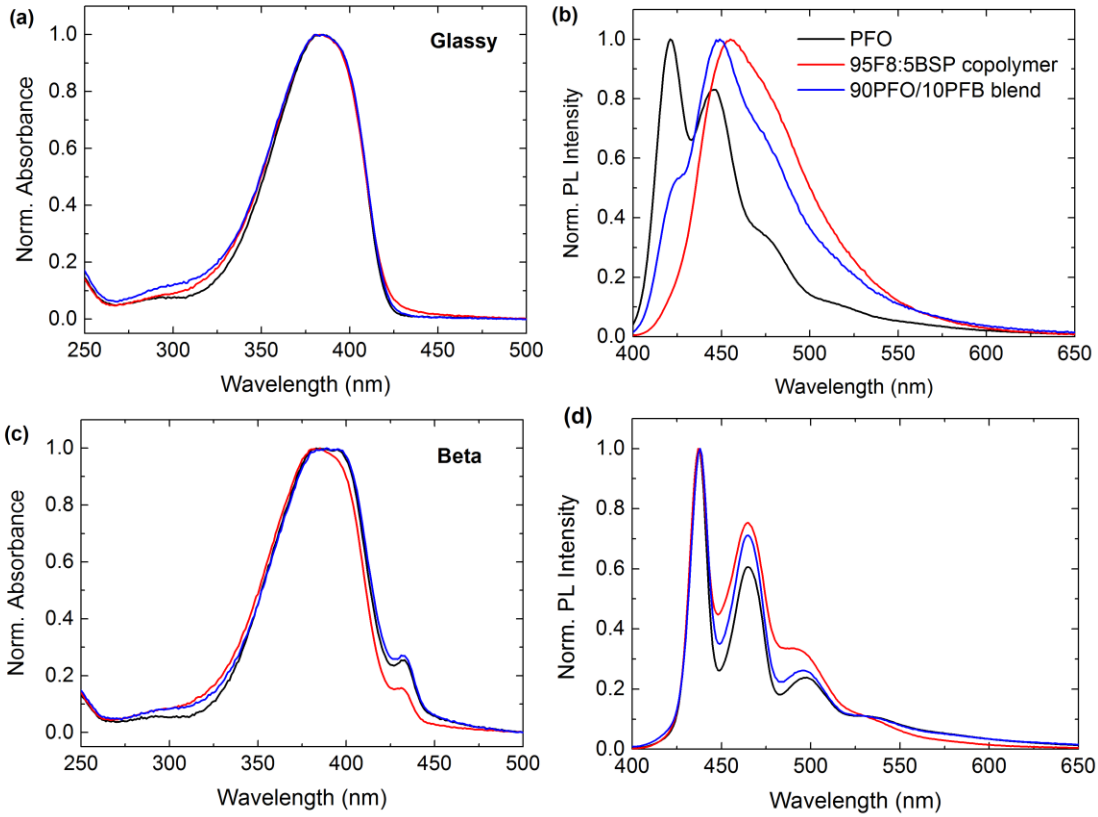

Figure S6. Peak normalised optical absorption ((a) and (c)) and PL emission (λ_{ex} = 385 nm) spectra ((b) and (d)) for PFO (black line), 95F8:5BSP copolymer (red line) and 90PFO/10PFB blend (blue line) films spin coated on spectrosil substrates. Glassy-phase data are shown in (a) and (b) whilst β-phase data are shown in (c) and (d). Spectra are overlaid for ease of comparison of the initial glassy-phase differences and the changes arising from β-phase chain segment formation within the three film types.

Time-correlated-single-photon-counting (TCSPC) PL decay measurements for PFO, 95F8:5BSP, 90PFO/10PFB and PFB

Thin film measurements

Figure S7 shows thin film TCSPC measurements (λ_{ex} = 404 nm) for glassy and β-phase microstructures of PFO, 95F8:5BSP and 90PFO/10PFB blend samples collected at range of wavelengths between 420-540 nm. PFO (glassy and β-phase) shows a bi-exponential decay made up of fast excitonic decay and slower, excimer-like decay from 'green-band' fluorenone defects.[S4] The latter decay increases in proportion at longer wavelength collections.

95F8:5BSP copolymer samples show decay times vary substantially with emission wavelength, with decay times increasing with wavelength collection rather than a change in component amplitude (as in PFO), suggesting a distribution of CT lifetimes within the copolymer.

The glassy 90PFO/10PFB blend sample shows a similar trend to the copolymer case, which is not surprising given that CT states from the PFB make up a significant fraction of the emission. β-phase 90PFO/10PFB TCSPC traces however shows a more PFO-like trend (redistribution of weights rather than lifetime as wavelength collection increases) as now excitonic PFO emission makes up the majority of PL emission.

PFB TCSPC traces (Figure S8) shows decay times increase with emission wavelength, as in the 95F8:5BSP copolymer case.

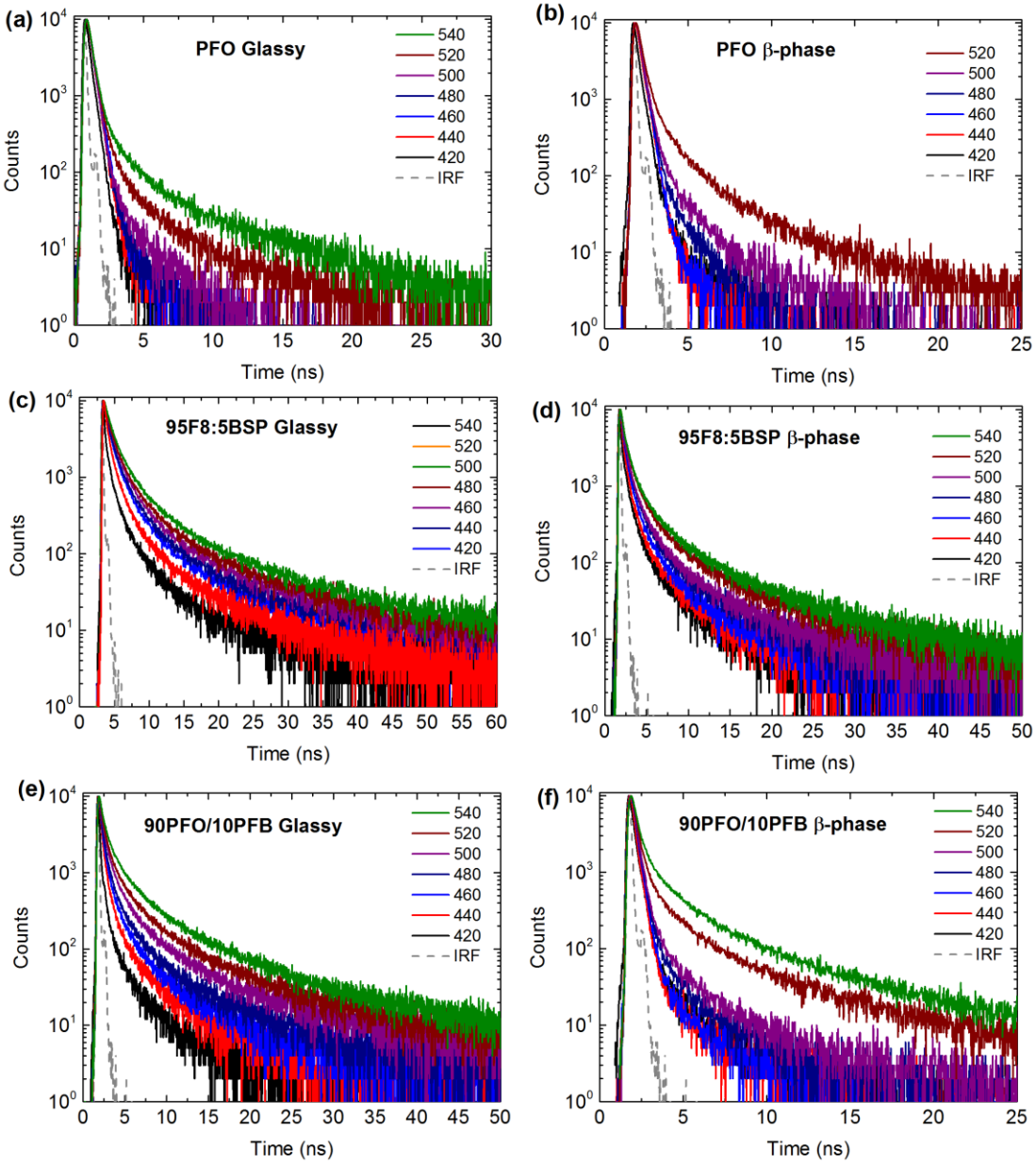

Figure S7. Thin film TCSPC decay curves (λ_{ex} = 404 nm) collected for the glassy- (left column) and β-phase (right column) microstructures of PFO ((a) and (b)), 95F8:5BSP ((c) and (d)) and 90PFO/10PFB ((e) and (f)). The dashed line is the instrument response function (IRF) and the decay curves from top to bottom run from long to short wavelengths (see legends for wavelength values in nm).

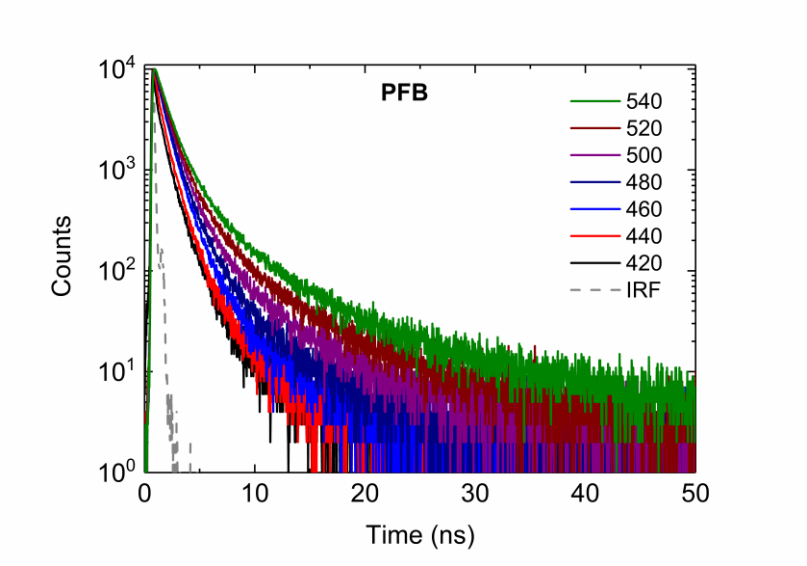

Figure S8. Thin film TCSPC decay curves for PFB. The dashed line is the instrument response function (IRF) and the decay curves from top to bottom run from long to short wavelengths (see legend for wavelength values in nm).

Solution measurements

Figure S9(a) shows the PL spectra of PFO, 95F8:5BSP and PFB in a dilute toluene solution, whilst parts (b)-(d) shows the solution TCSPC decay curves of PFO, 95F8:5BSP and PFB collected at 420-540 nm. PFO and PFB show mono-exponential decays at all collection wavelengths (~356 ps for PFO and ~1.4 ns for PFB) whilst the PL transients of the 95F8:5BSP copolymer in dilute solution (Figure S9(c)) show a bi-exponential decay at shorter wavelengths (420 and 440 nm), attributed to combined PFO-like excitonic emission (with τ_1 ~ 140 ps) and PFB-like CT emission (with τ_2 ~ 1.4 ns). At longer wavelengths, beyond 460 nm, a mono-exponential decay with $\tau \approx 1.4$ ns is observed, identical to the dilute solution decay for PFB.

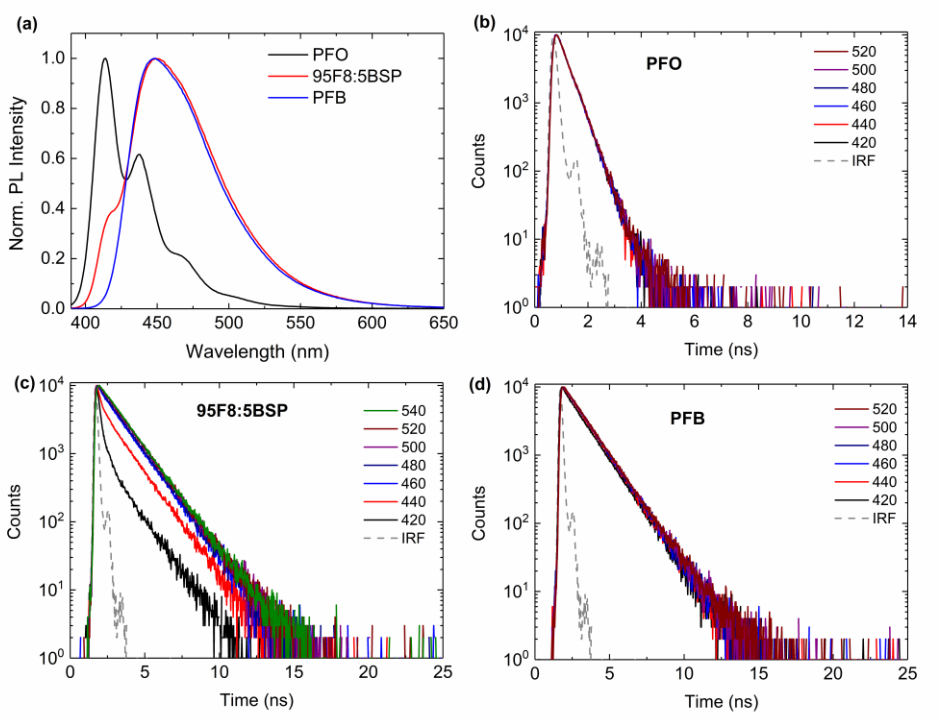

Figure S9. (a) PL emission spectra and ((b), (c), (d)) TCSPC decay curves for PFO, 95F8:5BSP and PFB in dilute (0.05 mg/ml) toluene solution. The homopolymer and alternating copolymer show single exponential decays whilst the sparse copolymer has more complex kinetics consistent with its two-component (PFO-like vibronic plus PFB-like CT) PL emission spectrum.

Deconvoluted electroluminescence spectra for 95F8:5BSP copolymer and 90PFO/10PFB blend β-phase EML devices

As for the PL spectra above, EL spectra from 95F8:5BSP copolymer and 90PFO/10PFB blend β-phase EML devices were deconvoluted to reveal the relative contributions of structured vibronic and CT-like emissions. The same procedure was applied to the EL data as used for PL.

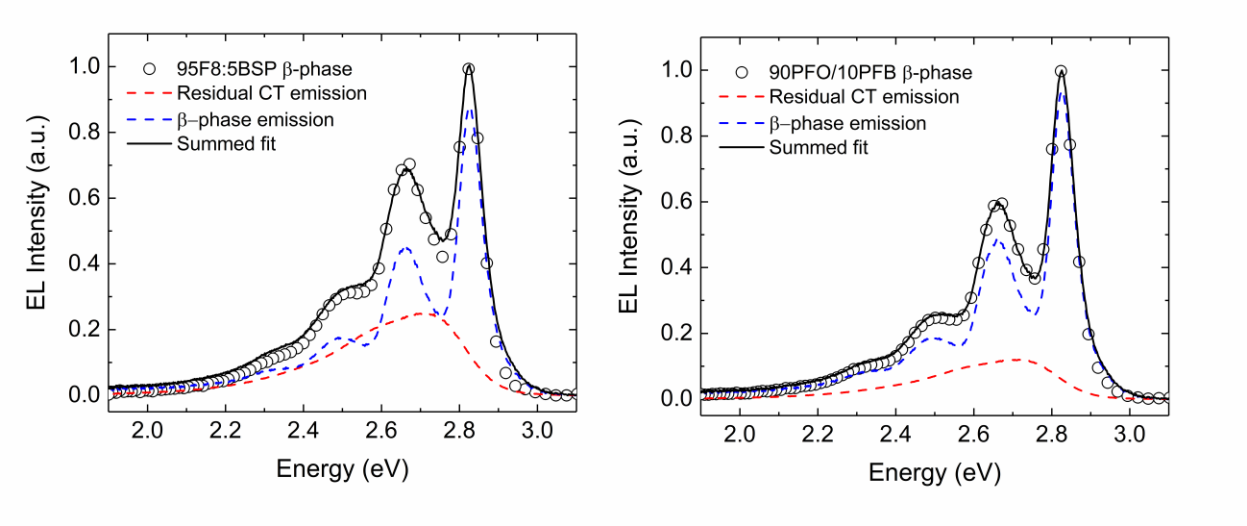

Figure S10. Deconvolution of EL spectra for 95F8:5BSP copolymer β-phase sample (left) and 90PFO/10PFB blend β-phase sample (right). The red dashed line shows residual PFB-like CT emission, whilst the blue dashed line shows the vibronic β-phase emission. The fractional contribution from each component was deduced by integration over their deconvoluted spectra.

AFM Topography images for PFO, 95F8:5BSP copolymer and 90PFO/10BSP blend films

Overall, the performance of the 90PFO/10PFB blend devices is poorer than for the 95F8:5BSP copolymer devices. It is clear that the volume fraction of BSP moieties is not the determining factor in this regard but the distribution of moieties within a polymer chain and through the bulk of a film also matter. In the blend, the BSP moieties are incorporated within PFB polymer chains at high density (alternating with 9,9-dioctylfluorene moieties) and these chains are then mixed with a majority (90%) of PFO polymer chains from which (at least partial) phase separation will occur. Evidence for phase separation is provided by the EL spectrum for glassy blend EML devices that shows a glassy PFO contribution (c.f. shoulder at ~ 425 nm on the blue edge of the spectrum) indicating incomplete energy transfer to PFB CT like emission sites. Atomic force microscopy (AFM) images for 60 nm thickness films of each EML are shown in Figure S11. Whilst the PFO and 95F8:5BSP films show largely featureless thin film microstructures (Figure S11 (a)-(d)), the 90PFO/10PFB blend films do indeed show phase separation between PFB and PFO chains in the glassy phase (Figure S11 (e)), with the image appearing to show ~10 nm raised islands through the film with a roughness of 1.32 nm. The β-phase blend thin film microstructure (Figure S11 (f)), however, appears to show ~10 nm sized recesses with a roughness of 1.76 nm. This suggests that whilst BSP units are evenly distributed through the 95F8:5BSP copolymer film, in the blend case the PFB chains are segregated, leading to less effective hole trapping which therefore leads to decreased device performance. In addition, β-phase segment formation by SVA has a more substantial effect on the EL spectrum of the blend EML devices than seen for 95F8:5BSP copolymer devices; deconvolution (Figure S10) indicates 80% β-phase emission and 20% CT emission compared to 66% β-phase and 34% CT emission for copolymer EML devices.

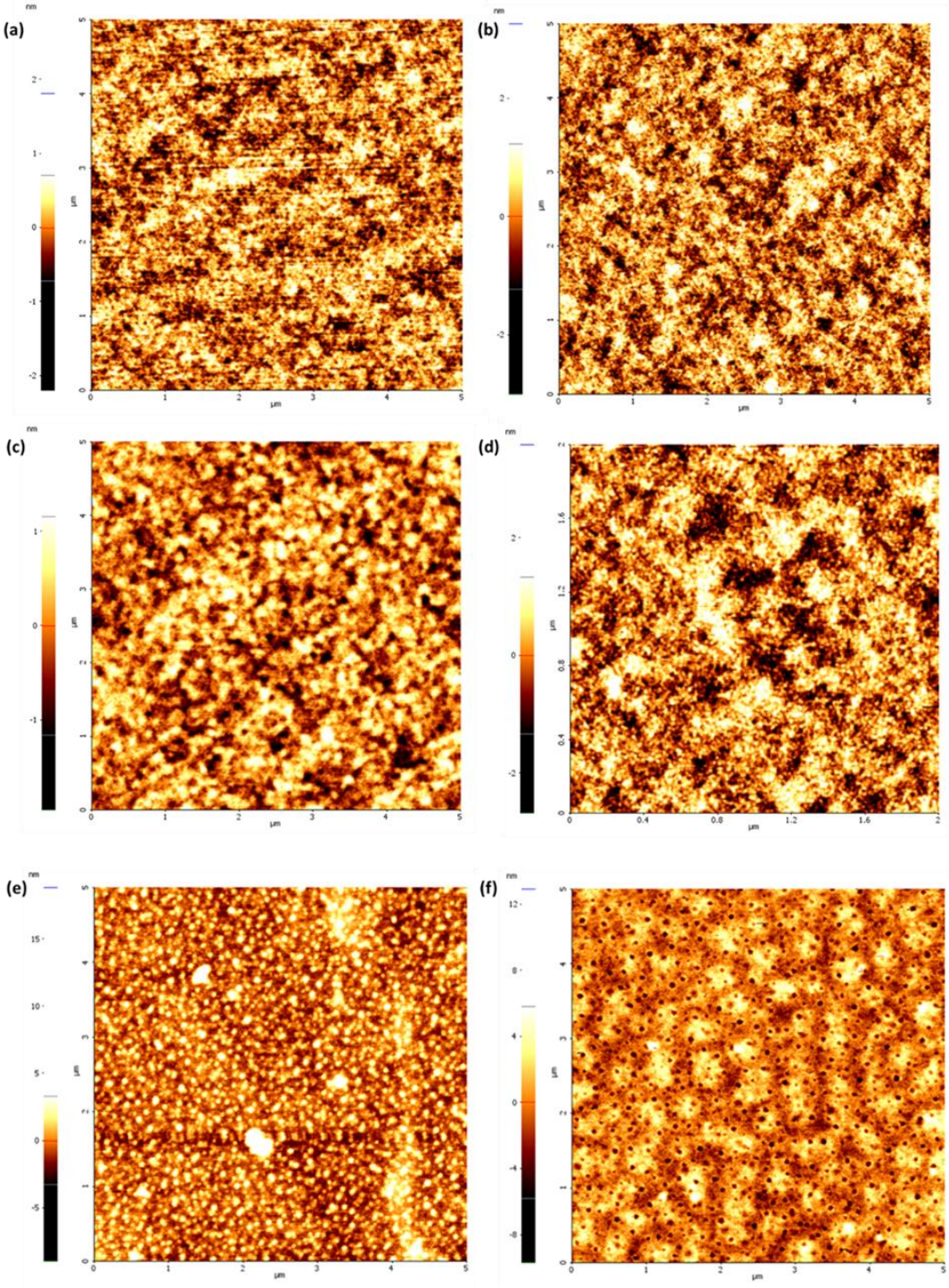

Figure S11. AFM topography images for glassy phase (left column) and β-phase (right column) microstructures of PFO ((a) and (b)), 95F8:5BSP copolymer ((c) and (d)) and 90PFO/10PFB blend ((e) and (f)) films.

Table S3. Root mean square roughness values (R_q) for PFO, 95F8:5BSP copolymer and 90PFO/10PFB blend films with glassy- and β-phase microstructures. The surface roughness for the blend is significantly higher than for the other two films. It is also generally the case that β-phase films are rougher than glassy ones.

Film Type	**Roughness, R_q (nm)**
PFO Glassy	0.349
PFO β-phase	0.627
95F8:5BSP Glassy	0.459
95F8:5BSP β-phase	0.680
90PFO/10PFB Glassy	1.319
90PFO/10PFB β-phase	1.763

97F8:3BSP and 90F8:10BSP copolymer PLED device data

PLED devices (ITO/PEDOT:PSS/TFB/copolymer EML/LiF/Ca/Al) were fabricated using 97F8:3BSP and 90F8:10BSP with both glassy and β-phase microstructures. J-V-L and efficiency (cd/A and lm/W) *vs* Voltage data are shown in Figure S12 and peak characteristics extracted therefrom are listed in Table S4. The 97F8:3BSP EMLs give good device performance with peak efficiencies of 3.4 cd/A and 2.4 lm/W for glassy and 3.1 cd/A and 2.0 lm/W for β-phase. The β-phase microstructure yields a slight drop in efficiency consistent with the behaviour for 95F8:5BSP copolymer and 90PFO/10PFB blend devices, however it also yields a desirable blue shift in emission from CIE(x, y) = (0.15, 0.17) to (0.15, 0.13). The EL spectra for both glassy and β-phase 97F8:3BSP EMLs are shown in Figure S13. The β-phase device shows strong S_1-S_0 vibronic emission with its 0-0 transition at 440 nm.

The 90F8:10BSP EML devices yielded poorer performance than 97F8:3BSP and 95F8:5BSP devices, with efficiencies of 1.7 cd/A and 0.6 lm/W for glassy and 1.3 cd/A and 0.4 lm/W for β-phase. We suggest that the increase in BSP content tends to reduce hole trapping, resulting in an increased hole-leakage current. The luminous efficiencies are again somewhat reduced for β-phase but as before there is a favourable blue shift in CIE (x, y) from (0.15, 0.16) to (0.15, 0.15); albeit that in this case the effect is less strong due to the lower fraction of vibronic emission that arises.

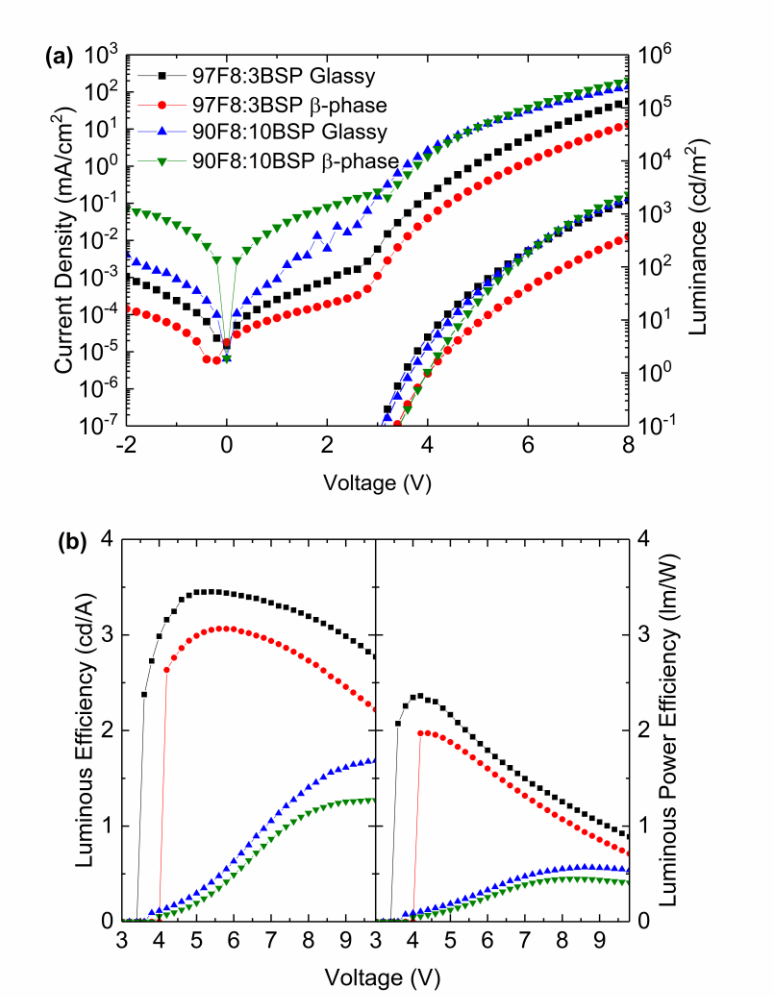

Figure S12. (a) J-V-L characteristics and (b) luminous and luminous power efficiencies for 97F8:3BSP and 90F8:10BSP copolymer PLEDs with glassy and β-phase emission layer (EML) microstructures. The device structures comprised ITO/PEDOT:PSS/TFB/copolymer EML/LiF/Ca/Al. Layer thicknesses are the same as those used in 95F8:5BSP copolymer devices, details of which are given in the experimental section of the main text.

Table S4. Summary of best PLED device performance data comprising 1 cd/m^2 turn-on (V), peak luminous efficiency (cd/A), peak power efficiency (lm/W) and CIE colour coordinates for 97F8:3BSP and 90F8:10BSP copolymer EMLs with glassy and β-phase microstructures.

EML Microstructure	EML copolymer	Turn on (V)	Peak Luminous efficiency (cd/A)	Peak Power efficiency (lm/W)	CIE (x, y)
Glassy	97F8:3BSP	3.6	3.4 @ 5.0 V	2.4 @ 4.2 V	(0.15, 0.17)
	90F8:10BSP	3.8	1.7 @ 9.8 V	0.6 @ 8.6 V	(0.15, 0.16)
β-phase	97F8:3BSP	4.0	3.1 @ 5.6 V	2.0 @ 4.4 V	(0.15, 0.13)
	90F8:10BSP	4.0	1.3 @ 9.6 V	0.4 @ 8.2 V	(0.15, 0.15)

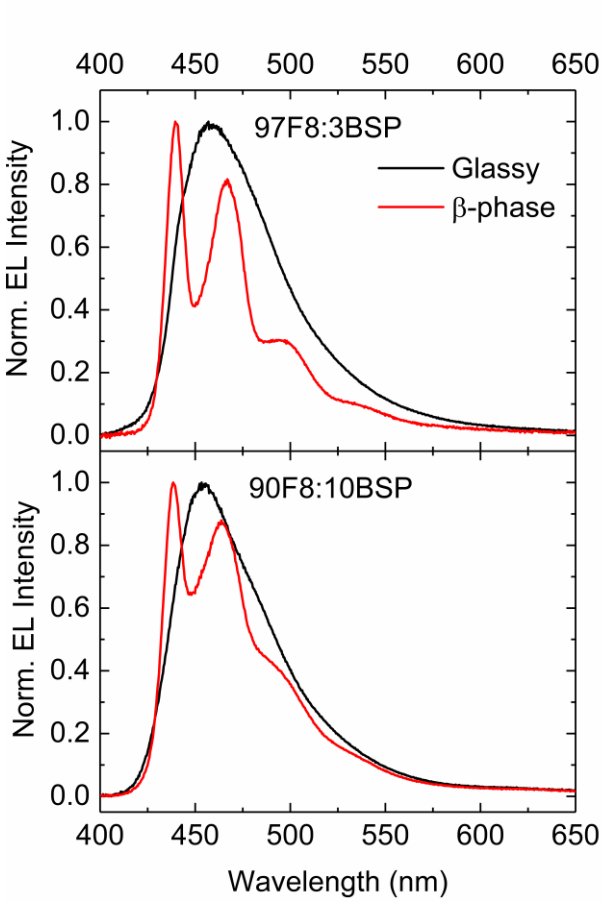

Figure S13. EL spectra for 97F8:3BSP and 90F8:10BSP copolymer PLEDs with glassy and β-phase EML microstructures.

95F8:5BSP PLED device lifetime

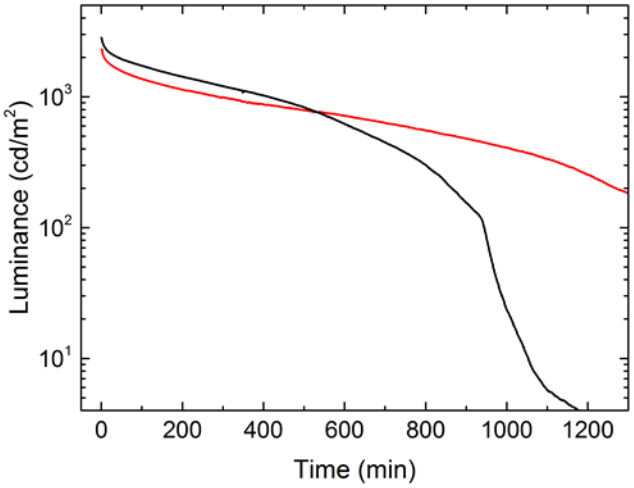

Figure S14. Accelerated luminance decay measurements for encapsulated 95F8:5BSP copolymer PLEDs driven at a constant current density J ≈ 90 mA/cm^2. Results are shown for both glassy (black line) and β-phase (red line) EML devices.

Both pre- and post-SVA 95F8:5BSP EML PLEDs were subjected to accelerated lifetime testing using a constant current source set to deliver 4 mA (i.e. J ≈ 90 mA/cm^2 for the 4.44 mm^2 pixels under test). The luminance was measured at 60-second intervals starting from 2821 cd/m^2 for glassy- and 2300 cd/m^2 for β-phase devices. Initially (Figure S14), the glassy and β-phase EML PLED luminance values decayed at a similar rate, with half decay times $T_{50\%}$ (glassy) = 176 mins and $T_{50\%}$ (β-phase) = 180 mins. The subsequent decay was much more rapid in the glassy copolymer EML devices, especially beyond 400 mins. The luminance took 490 mins to drop to 30% of its starting value for the glassy 95F8:5BSP EML PLED, but took 630 mins to reach the same fractional output for the β-phase device. In addition, whilst the latter was still emitting some 250 cd/m^2 at 1200 mins the glassy device luminance had fallen below 4 cd/m^2 by that time. The

operational stability of the β-phase 95F8:5BSP copolymer EML device is clearly significantly greater than for the corresponding glassy-phase device.

It is expected that the initial luminance decay is caused by degradation of the reactive LiF and Ca layers in the composite cathode that is used for both device types. The subsequent degradation is slower for the β-phase EML structures for which the emission is dominated by F8 centred excitonic states. In addition to the known stabilising effect of β-phase on extended F8 sequences,[S5] this difference suggests a reduced stability for the BSP moiety centred CT like states that dominate emission from glassy copolymer EML structures.

In summary, therefore, induction of β-phase chain segments in 95F8:5BSP copolymer EMLs not only improves PLED CIE coordinates, but also operational lifetime.

Low temperature photoluminescence measurements

Figure S15 (a) shows that as the PFO β-phase sample decreases in temperature, the PL spectra red shifts by ~ 5 nm whilst the 0-0 linewidth decreases by some ~35 meV which has been previously linked to increases in β-phase conjugation length and planarity.[S6] The 0-1 and 0-2 vibronics show distinctive splitting into at least three peaks. Figure S15(b) shows the glassy 95F8:5BSP copolymer emission reduces in linewidth as temperature decreases, with the spectra resolving into a main high energy peak at ~454 nm with a lower energy shoulder at ~478 nm. Low temperature β-phase 95F8:5BSP PL measurements (Figure S15(c) and (d)) reveal the spectra remains a superposition of both the vibronic β-phase emission and a CT-like emission from BSP centered states from 10–290 K. Spectral deconvolution reveals the component spectra appear identical to either the PFO β-phase or the glassy 95F8:5BSP spectra at each particular temperature, an example of which is shown in Figure S15(e) for 10 K. By integrating the component spectra at each temperature we find that (Figure S15(f)) the fraction of β-phase emission decreases as temperature decreases, from ~64% at 290 K to ~32% at 10 K.

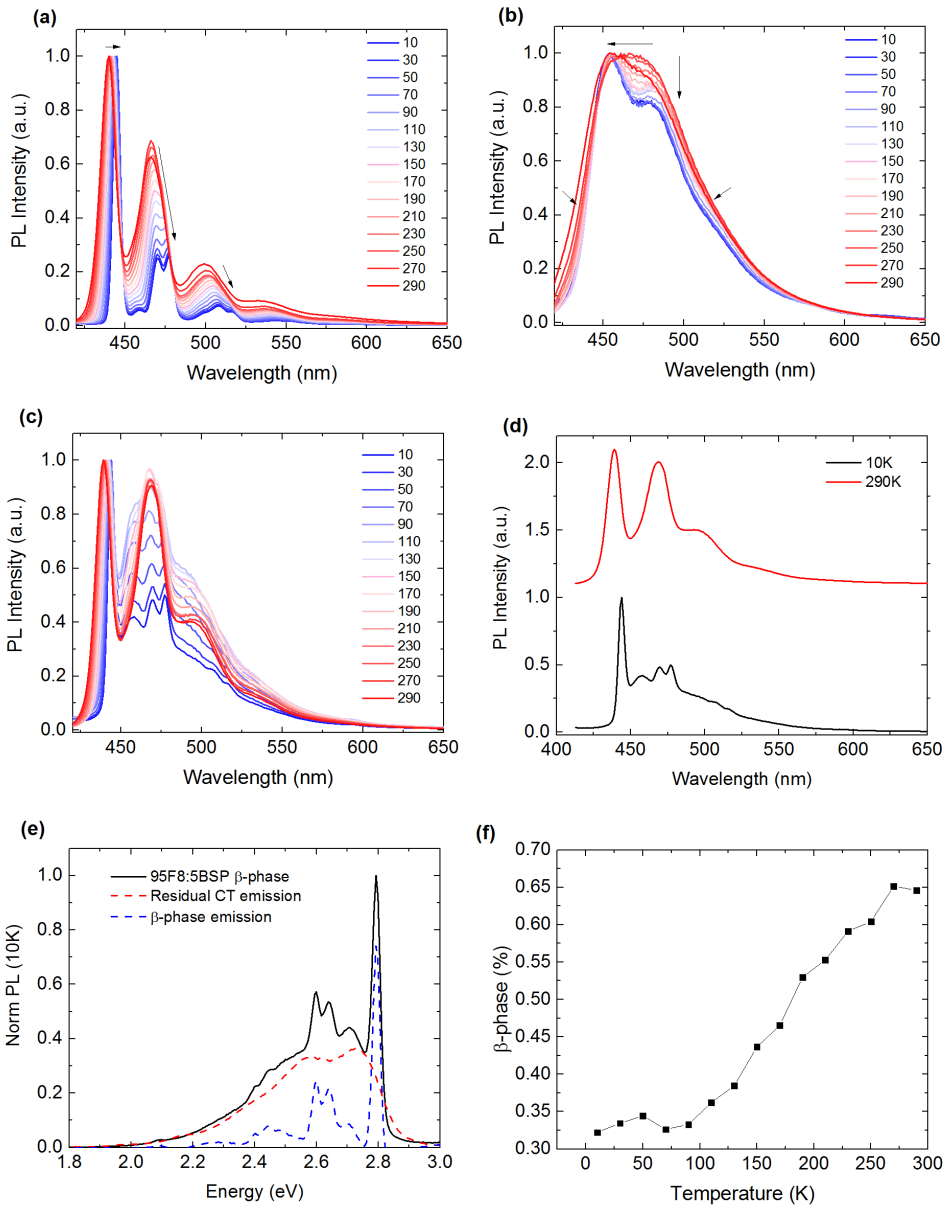

Figure S15. Photoluminescence spectra (λ_{ex} = 400 nm) of (a) β-phase PFO, (b) glassy phase 95F8:5BSP and (c) β-phase 95F8:5BSP samples at a temperature range of 10 to 290 K. Panel (d) shows the β-phase 95F8:5BSP spectra at 10 K and 290 K and (e) shows the deconvolution of the 10 K β-phase 95F8:5BSP spectra into the component β-phase and residual CT emission. Panel (f) shows the percentage fraction of β-phase emission as a function of temperature.

Voltage dependent EL spectra for a ~95 nm thick 95F8:5BSP β-phase PLED

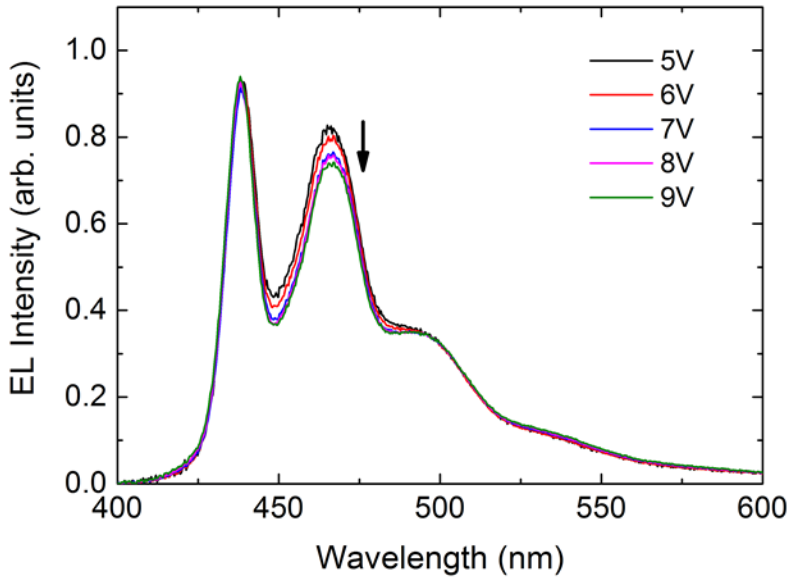

Figure S16. Voltage dependent EL spectra for a β-phase 95F8:5BSP PLED with an EML layer thickness of ~95 nm. The fraction of residual CT like emission appears to reduce with increasing voltage as BSP sites become saturated and β-phase F8 segments become filled with excited species. This can be seen by a reduction in intensity between 445-495 nm with increasing voltage.

Energy transfer mechanism in 90PFO/10PFB blend films and PLEDs

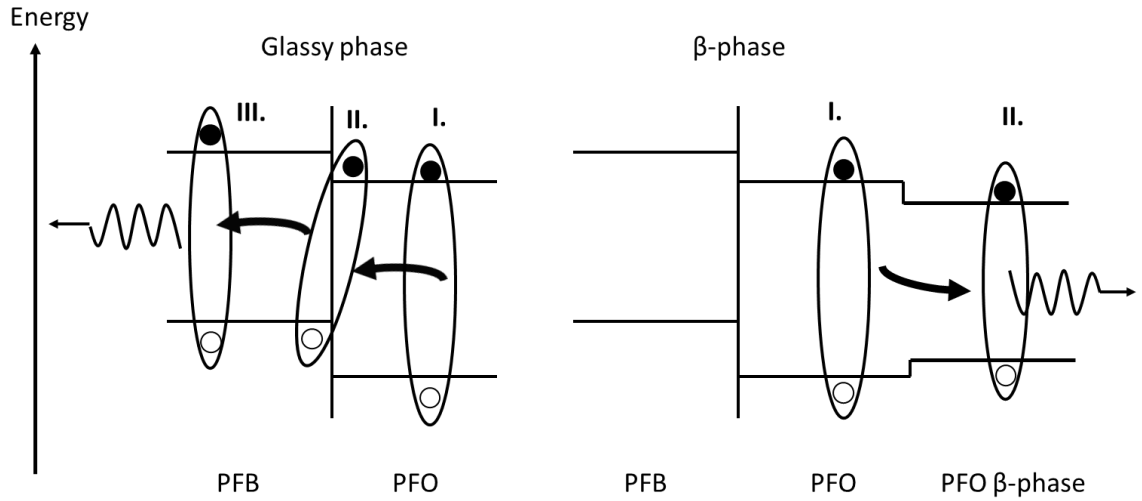

Figure S17. Diagram showing anticipated energy transfer in 90PFO/10PFB blend films after optical excitation of glassy PFO chain segments.

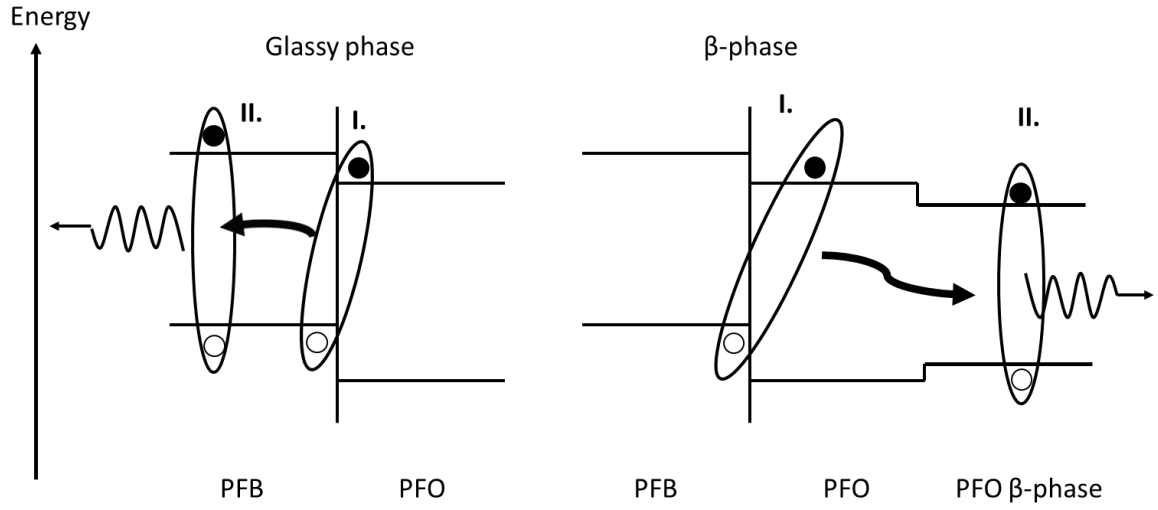

Figure S18. Diagram showing anticipated energy transfer mechanism in 90PFO/10PFB blend after electrical excitation forms a PFB:PFO exciplex state.

References

(S1) Perevedentsev, A.; Chander, N.; Kim, J.-S.; Bradley, D. D. C. Spectroscopic Properties of poly(9,9-Dioctylfluorene) Thin Films Possessing Varied Fractions of β-Phase Chain Segments: Enhanced Photoluminescence Efficiency via Conformation Structuring. *J. Polym. Sci. Part B Polym. Phys.* **2016**, *54*, 1995–2006.

(S2) Janietz, S.; Bradley, D. D. C.; Grell, M.; Giebeler, C.; Inbasekaran, M.; Woo, E. P. Electrochemical Determination of the Ionization Potential and Electron Affinity of poly(9,9-Dioctylfluorene). *Appl. Phys. Lett.* **1998**, *73* (17), 2453–2455.

(S3) Sekine, C.; Tsubata, Y.; Yamada, T.; Kitano, M.; Doi, S. Recent Progress of High Performance Polymer OLED and OPV Materials for Organic Printed Electronics. *Sci. Technol. Adv. Mater.* **2014**, *15* (3), 34203.

(S4) Chan, K. L.; Sims, M.; Pascu, S. I.; Ariu, M.; Holmes, A. B.; Bradley, D. D. C. Understanding the Nature of the States Responsible for the Green Emission in Oxidized poly(9,9-Dialkylfluorene)s: Photophysics and Structural Studies of Linear Dialkylfluorene/fluorenone Model Compounds. *Adv. Funct. Mater.* **2009**, *19* (13), 2147–2154.

(S5) Arredondo, B.; Romero, B.; Gutiérrez-Llorente, A.; Martínez, A. I.; Álvarez, A. L.; Quintana, X.; Otón, J. M. On the Electrical Degradation and Green Band Formation in α- And β-Phase poly(9,9-Dioctyfluorene) Polymer Light-Emitting Diodes. *Solid. State. Electron.* **2011**, *61* (1), 46–52.

(S6) Ariu, M.; Sims, M.; Rahn, M. D.; Hill, J.; Fox, A. M.; Lidzey, D. G.; Oda, M.; Cabanillas-Gonzalez, J.; Bradley, D. D. C. Exciton Migration in β-Phase poly(9,9-Dioctylfluorene).

Phys. Rev. B **2003**, *67* (19), 195333.